INTERNATIONAL JOURNAL OF HYDROGEN ENERGY XXX (2017) 1–10

Available online at www.sciencedirect.com

ScienceDirect

journal homepage: www.elsevier.com/locate/he

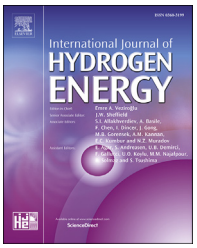

$Ni/Ce_{0.95}M_{0.05}O_{2-d}$ (M = Zr, Pr, La) for methane steam reforming at mild conditions

Ignacio Iglesias[*], *Graciela Baronetti*, *Fernando Mariño*

Laboratorio de Procesos Catalíticos, Dpto. de Ingeniería Química, ITHES (UBA-CONICET), Universidad de Buenos Aires, Ciudad Autónoma de Buenos Aires, Argentina

ARTICLE INFO

Article history:
Received 4 August 2017
Received in revised form
9 September 2017
Accepted 30 September 2017
Available online xxx

Keywords:
Methane reforming
Nickel
Ceria
Doped ceria

ABSTRACT

Methane obtained from renewable resources such as biogas or biomass gasification may be reformed to produce hydrogen, an important and environmentally friendly energy vector. In the present work, nickel based catalysts supported on either pure or doped ceria (5 at% of Zr, Pr or La doping) were studied for this purpose. Catalysts were obtained by impregnation of 5 wt% nickel of ceria based supports prepared by coprecipitation by the urea method. Catalysts were calcined at three temperatures (600, 750 or 900 °C), characterized by different techniques (XRD, H_2-TPR, TPO, OSC-OSCC, H_2-Chemisorption) and evaluated at different feed conditions and temperatures for methane steam reforming. Catalysts calcined at 900 °C were tested at three different reaction temperatures (600, 700 and 800 °C). Higher temperatures favored methane conversion and CO selectivity. For catalysts tested at 600 °C, increasing vapor/methane ratio caused an increase in hydrogen yield and lowered carbon formation. However, high vapor pressure was seen to favor nickel sintering. Intermediate calcination temperature (750 °C) enhanced nickel-support interaction leading to maximum methane conversion.

Introduction

In the last decades, fossil fuels depletion and increasing environmental consciousness led to much work in the pursuit of alternative energy sources, i.e. renewable and environmentally friendly ones. In this line, hydrogen was recognized as an interesting energy vector since its combustion has water vapor as only sub product [1,2]. Furthermore, hydrogen may be fed to a fuel cell where energy conversion is not limited by Carnot efficiency for internal combustion engines [3]. Despite having higher energy per mass compared to other fuels, due to H_2 low density, high pressures or volumes are required for its storage. Therefore, in situ production is mandatory.

Among hydrogen production technologies, one of the most studied approaches to obtain hydrogen in situ is methane steam reforming (MSR) (Equation (1)) which is accompanied by water gas shift equilibrium reaction (WGS) (Equation (2)) [4]:

$$CH_4 + H_2O \rightarrow CO + 3H_2 \quad \Delta H^0_{298K} = 206 kJ/mol \tag{1}$$

$$CO + H_2O \rightarrow CO_2 + H_2 \quad \Delta H^0_{298K} = -41 kJ/mol \tag{2}$$

It should be noted that hydrogen will be as environmentally friendly as its source is. In consequence, instead of natural gas, renewable methane sources such as biogas and biomass gasification could be considered. Both biogas, which is obtained as a result of anaerobic degradation of biomass [5]

* *Corresponding author.*
E-mail address: ignacio.d.iglesias@gmail.com (I. Iglesias).

https://doi.org/10.1016/j.ijhydene.2017.09.176

Please cite this article in press as: Iglesias I, et al., $Ni/Ce_{0.95}M_{0.05}O_{2-d}$ (M = Zr, Pr, La) for methane steam reforming at mild conditions, International Journal of Hydrogen Energy (2017), https://doi.org/10.1016/j.ijhydene.2017.09.176

and the exit current of biomass gasification contain mainly methane, carbon oxides and some light hydrocarbons [6]. Since the aim of this work is to reform this type of current, methane was chosen as a representative molecule because its stable chemical structure makes it the most difficult compound to reform [7].

Given that MSR is a well known industrial process, catalysts for this reaction were widely studied. Between these, nickel catalysts are preferred because of their reasonable high activity and low cost compared to noble metal formulations [8,9]. Nickel is usually supported on alumina based materials because of their high thermal and mechanical stability [10,11]. Being MSR reaction endothermic and having a positive change in total moles number, both moderate pressures (typically 20 bar) and high temperatures (over 750 °C) are employed to attain high conversion. In addition, since coking deactivation problems are frequent when using nickel based catalysts, high water/methane ratios are usually employed to favor gasification reactions, i.e. water/methane ratios over 3 [12]. All conditions mentioned have a high cost associated for the MSR process which is desirable to lower [13]. Therefore, new materials are being studied to work at mild conditions: low pressure, temperature and water vapor pressure [14,15].

In this work, nickel was chosen as active metal and ceria based materials as supports. High oxygen mobility, characteristic of ceria, was proven to enhance gasification reactions which diminish carbon deposits on the catalysts [16–18]. Furthermore, oxygen mobility may be enhanced by doping ceria with even small quantities of other elements [19]. Catalysts prepared in the present work, containing 5 wt% of Ni supported on pure or doped ceria: 5 at% of Zr, Pr or La, were characterized and evaluated in different reaction conditions to identify possible deactivation phenomena, best operation conditions and dopant effects on catalyst structure and activity.

Materials and methods

Sample preparation

Supports were prepared by coprecipitation method employing the homogeneous thermal decomposition of urea [20], being the doping percentage (Zr, Pr, La) 5 %at in every case. Aqueous solutions of urea, ceria and dopant nitrates were prepared with urea/cations ratio 10/1 and kept at 90 °C for 24 h. The precipitate obtained was washed and centrifuged three times before drying at 80 °C overnight. Afterwards, the solid was calcined at the desired temperature (600, 750 or 900 °C) for 5 h in muffle. Supports prepared were named CeM_5T (M = La, Pr, Zr and T = 600, 750, 900) where number five refers to the atomic percentage of the dopant M and T indicates calcination temperature in °C. Supports were then impregnated with a nickel nitrate solution which concentration was established to obtain 5 wt% of Ni in the catalysts. After impregnation, the solids were dried at 80 °C overnight and finally calcined at the desired temperature (600, 750 or 900 °C) for 5 h in muffle. The catalysts were named 5% Ni/CeM_5 T, consistently with support's nomenclature.

Sample characterization

XRD measurements were conducted in a Siemens D-501 diffractometer with Johansson Ge (1 1 1) monochromator, CuK alpha radiation, 45 kV and 35 mA. Micromeritics AutoChem II was used for H_2-TPR, TPO, OSC-OSCC and H_2-Chemisorption measurements. Before starting any of these measurements, the solid surface was cleaned by flowing air at 450 °C for 30 min to eliminate any carbonates or adsorbed impurities usually present in these samples [21].

For H_2-TPR, mass employed was 30 mg, total gas flow 50 Nml/min (4% H_2/Ar) and temperature was raised from ambient to 1000 °C at 10 °C/min. For TPO analysis total gas flow 50 Nml/min (5% O_2/Ar) and temperature was raised from ambient to 1000 °C at 10 °C/min. For OSC (Oxygen Storage Capacity) and OSCC (Oxygen Storage Capacity Complete) measurements at isothermal conditions (400 °C), the traditional method described by Yao and YuYao was followed [22]. In first place, alternate pulses of oxidant (air) and reductant (5% CO/Ar) were injected until stable CO_2 production was registered (OSC), i.e. typically 10 pulses. Afterwards, successive reductant pulses were injected until no CO_2 production was registered (OSCC). For H_2-Chemisorption experiments, following the oxidizing pretreatment mentioned, the sample was reduced at 500 °C with 50 Nml/min (4% H_2/Ar) until no H_2 consume was detected. Afterwards, sample was cooled down with purified Ar flow (CRS ZPure Glass Oxygen Purifier) up to −80 °C, temperature employed for pulse injection to avoid support's concomitant reduction, following conditions established by Hennings and Reimert [23].

Samples catalytic evaluation

Activity tests were carried out in an isothermal tubular fixed bed reactor where temperature was measured by a K-type thermocouple placed at the center of the catalyst bed. High purity gases provided by Air Liquide were fed by Aalborg mass flow controllers and gas mixture composition, both at the entrance and the exit of reactor, was analyzed by gas chromatography employing a Shimadzu GC 14-B chromatograph equipped with TCD (thermal conductivity detector) and FID (flame ionization detector). Before each activity test, the catalysts were pretreated with 5% H_2 in N_2 at 500 °C for 60 min before rising the temperature in N_2, up to the desired reaction temperature (600 °C, 700 °C or 800 °C). All catalytic tests were performed with constant contact time (W = 100 mg, F = 100 Nml/min, W/F = 1 g min/Nml) and the following composition at reactor entrance: CH_4 (12.5%), H_2O/CH_4 (0.5, 1, 1.5 or 3) and N_2 as balance. Time-on-stream was 4 h for every catalytic test since this period was enough for methane conversion, CO and CO_2 selectivities stabilization. Values reported on Tables 4–6 are all average values in this period. Supports activity in MSR was tested and resulted negligible. Methane conversion, CO and CO_2 selectivities and H_2 yield were calculated by their usual definitions:

$$x_{CH_4} = \frac{F^{in}_{CH_4} - F_{CH_4}}{F^{in}_{CH_4}} \quad (3)$$

Please cite this article in press as: Iglesias I, et al., Ni/$Ce_{0.95}M_{0.05}O_{2-d}$ (M = Zr, Pr, La) for methane steam reforming at mild conditions, International Journal of Hydrogen Energy (2017), https://doi.org/10.1016/j.ijhydene.2017.09.176

Table 1 – BET, XRD, OSC-OSCC and H_2-TPR results for supports calcined at different temperatures.

Support	S_{BET} ($m^2\ g^{-1}$)	d_{CeO2} (nm)	a_{XRD} (Å)	OSC (μmol CO_2/g)	OSCC (μmol CO_2/g)	Total H_2 uptake (μmol/g)
CeO_2 600	53.8	21	5.411 (5.410)	48	123	1273
CeO_2 750	8.0	41		27	85	1063
CeO_2 900	6.0	79		19	34	863
$CeLa_5$ 600	49.0	17	5.426 (5.428)	48	122	789
$CeLa_5$ 750	12.0	29		30	65	530
$CeLa_5$ 900	8.6	50		19	36	517
$CePr_5$ 600	49.6	21	5.412 (5.413)	63	147	1543
$CePr_5$ 750	10.9	38		76	165	911
$CePr_5$ 900	5.5	65		56	149	634
$CeZr_5$ 600	44.8	25	5.399 (5.410)	82	202	1141
$CeZr_5$ 750	14.8	37		55	123	770
$CeZr_5$ 900	10.6	43		38	80	536

Table 2 – XRD, OSC-OSCC and H_2-Chemisorption results for catalysts calcined at different temperatures.

Catalyst	$d_{XRD\ NiO}$ (nm)	OSC (μmol CO_2/g)	OSCC (μmol CO_2/g)	A_{Ni} (m^2 Ni/g)
5% Ni/CeO_2 600	24	123	409	0.76
5% Ni/$CeLa_5$ 600	25	123	492	0.73
5% Ni/$CePr_5$ 600	26	164	633	0.46
5% Ni/$CeZr_5$ 600	27	209	661	1.58
5% Ni/CeO_2 750	40	120	398	0.69
5% Ni/$CeLa_5$ 750	33	99	396	0.34
5% Ni/$CePr_5$ 750	36	110	426	0.74
5% Ni/$CeZr_5$ 750	34	129	409	1.10
5% Ni/CeO_2 900	42	115	382	0.18
5% Ni/$CeLa_5$ 900	40	93	373	0.06
5% Ni/$CePr_5$ 900	40	103	400	0.10
5% Ni/$CeZr_5$ 900	37	122	384	0.23

$$S_{CO} = \frac{F_{CO} - F_{CO}^{in}}{F_{CH_4}^{in} - F_{CH_4}} \quad (4)$$

$$S_{CO_2} = \frac{F_{CO_2} - F_{CO_2}^{in}}{F_{CH_4}^{in} - F_{CH_4}} \quad (5)$$

$$S_C = 1 - S_{CO} - S_{CO_2} \quad (6)$$

$$Y_{H_2} = \frac{x_{CH_4}(4S_{CO_2} + 3S_{CO})}{4} \quad (7)$$

Additionally, in order to quantify catalyst deactivation, methane conversion diminution during 4 h time-on-stream was calculated by:

$$\phi = 1 - x_{CH_4}(4h) \Big/ x_{CH_4}^0 \quad (8)$$

where $x_{CH_4}(4h)$ is methane conversion after 4 h on stream and $x_{CH_4}^0$ is methane initial conversion. As it is observed from Equation (8), α equals 1 when deactivation is complete and 0 if there is no deactivation.

Results and discussion

Characterization results

The supports employed were thoroughly characterized by various techniques (BET, XRD, Raman spectroscopy, H_2-TPR, OSC-OSCC). Relevant results for the discussion in the present

Table 3 – H_2-TPR profiles deconvolution results for catalysts calcined at different temperatures.

Catalyst	Peak α	Peak β	Peak ϒ	Peak δ	Peaks α + β + ϒ H_2 uptake (μmol/g	Peak δ H_2 uptake (μmol/g	Total H_2 uptake (μmol/g)
	Position (°C)	Position (°C)	Position (°C)	Position (°C)			
5% Ni/Ce 600	266	281	323	803	831	1579	2409
5% Ni/$CeLa_5$ 600	276	309	369	767	1219	988	2207
5% Ni/$CePr_5$ 600	194, 234	318	358	766	917	968	1885
5% Ni/$CeZr_5$ 600	256	338	367	827	489	1599	2088
5% Ni/Ce 750	258	334	363	797	901	2888	3789
5% Ni/$CeLa_5$ 750	260	316	348	693	1232	1947	3180
5% Ni/$CePr_5$ 750	222, 262	340	384	744	1122	1636	2760
5% Ni/$CeZr_5$ 750	220	287	308	733	868	1940	2808
5% Ni/Ce 900	–	319	344	770	917	1335	2252
5% Ni/$CeLa_5$ 900	240	310	343	714	1446	1253	2699
5% Ni/$CePr_5$ 900	234, 256	331	365	729	1130	1332	2461
5% Ni/$CeZr_5$ 900	205	332	386	770	1039	1199	2238

Please cite this article in press as: Iglesias I, et al., Ni/$Ce_{0.95}M_{0.05}O_{2-d}$ (M = Zr, Pr, La) for methane steam reforming at mild conditions, International Journal of Hydrogen Energy (2017), https://doi.org/10.1016/j.ijhydene.2017.09.176

Table 4 – Catalytic results of catalysts calcined at 900 °C evaluated at different reaction temperatures. (R = 1, W/F = 1 g min/Nml, Time-on-stream = 4 h).

Catalyst	T (°C)	x_{CH_4} (%)	S_{CO} (%)	S_{CO_2} (%)	φ (%)
5% Ni/Ce 900	600	39	44	46	25
	700	66	61	18	35
	800	71	77	16	31
5% Ni/$CeLa_5$ 900	600	60	57	33	22
	700	63	64	18	20
	800	76	76	7	20
5% Ni/$CePr_5$ 900	600	42	38	53	30
	700	49	64	19	34
	800	56	73	15	29
5% Ni/$CeZr_5$ 900	600	54	54	38	27
	700	64	69	26	23
	800	67	73	13	40

Table 5 – Catalytic results of catalysts calcined at 600 °C evaluated at different water/methane feed ratios (R). (T = 600 °C, W/F = 1 g min/Nml, Time-on-stream = 4 h).

Catalyst	x_{CH_4} (%)	S_{CO} (%)	S_{CO_2} (%)	Y_{H_2} (%)	φ (%)
R = 0.5					
5% Ni/Ce 600	27	57	22	17	56
5% Ni/$CeLa_5$ 600	27	61	30	20	26
5% Ni/$CePr_5$ 600	29	61	21	20	51
5% Ni/$CeZr_5$ 600	36	56	20	23	48
R = 1					
5% Ni/Ce 600	51	51	28	34	31
5% Ni/$CeLa_5$ 600	52	47	35	37	9
5% Ni/$CePr_5$ 600	51	58	34	43	27
5% Ni/$CeZr_5$ 600	39	50	38	29	19
R = 1.5					
5% Ni/Ce 600	70	49	36	51	9
5% Ni/$CeLa_5$ 600	54	49	34	38	2
5% Ni/$CePr_5$ 600	68	43	39	48	3
5% Ni/$CeZr_5$ 600	60	39	42	43	7
R = 3					
5% Ni/Ce 600	55	39	56	47	22
5% Ni/$CeLa_5$ 600	67	39	49	53	5
5% Ni/$CePr_5$ 600	72	42	52	60	15
5% Ni/$CeZr_5$ 600	72	59	41	70	13

Table 6 – Catalytic results of catalysts calcined at different temperatures and evaluated at 600 °C and R = 1. (T = 600 °C, R = 1, W/F = 1 g min/Nml, Time-on-stream = 4 h).

Catalyst	Calcination temperature (°C)	x_{CH_4} (%)	S_{CO} (%)	S_{CO_2} (%)	Y_{H_2} (%)	φ (%)
5% Ni/Ce	600	51.1	51.4	28.0	34.0	31
	750	57.4	55.4	31.6	42.0	30
	900	39.3	43.8	46.2	31.1	25
5% Ni/$CeLa_5$	600	52.1	47.3	35.3	36.9	9
	750	58.4	53.7	31.9	42.1	8
	900	59.5	56.7	32.8	44.8	22
5% Ni/$CePr_5$	600	51.2	57.8	33.7	42.5	27
	750	61.7	55.1	29.7	43.9	27
	900	42.1	38.2	52.7	34.3	30
5% Ni/$CeZr_5$	600	38.5	49.9	38.0	29.0	19
	750	62.0	52.8	29.3	42.7	18
	900	54.3	54.2	38.3	42.9	27

work are summarized in Table 1 while details and further analysis can be found in our previous work [24].

Fig. 1 shows the measured XRD patterns for catalysts precursors calcined at different temperatures. In addition to ceria fluorite structure reflections (JCPDS 34-0394), nickel oxide was detected (JCPDS 47-1049) in every catalyst precursor.

Lattice parameters determined from these diffractograms (indicated between parentheses below supports' values in Table 1) were not significantly different from those observed for the supports. Therefore Ni^{2+} insertion in the lattice was discarded since it would have produced noticeable contraction because of its smaller ionic radii, as reported in literature [25,26].

The (2 0 0) reflection located at $2\theta = 43.2°$ was used for nickel oxide crystallite diameter determination because of its highest intensity in accordance with other authors [27,28]. Calculated values, presented in Table 2, are in line with previous reports by other authors: Huang & Huang [29] obtained 25 nm NiO particles using 5 %wt. supported on Gd-doped ceria and Radlik et al. [30] obtained 17 nm particles with 550 °C-calcined samples. It may be observed that for calcination temperatures over 600 °C, doped samples had smaller crystallite sizes, specially the one supported on Zr-doped ceria. These observations are accordance with metallic area results also shown in Table 2 and discussed below in this section.

Fig. 2 shows the catalysts' reduction profiles and deconvolution results are presented in Table 3. Two temperature regions can be distinguished: high temperature region is again identified with bulk ceria reduction (Peak δ) while in the low temperature region both labile oxygen and nickel oxide reduction events are lumped (Peaks α, β and ϒ) [31–35]. Considering the following reaction for nickel oxide reduction:

$$NiO + H_2 \rightarrow H_2O + Ni^0 \quad (9)$$

The amount of hydrogen consumed for complete nickel oxide reduction can be calculated as 852 μmol/g. Therefore, taking into consideration the values in Tables 1 and 3, simultaneous ceria and nickel reduction can be assumed in the low temperature region.

Furthermore, it can be observed that bulk ceria reduction is enhanced by nickel impregnation as previously reported by other authors [36]. Given that nickel reduces in one step from Ni^{2+} to Ni^0, separate reduction events (Peaks β and ϒ) are usually ascribed to two different nickel particles: dispersed and agglomerated ones [37]. In addition, Peak α is attributed to highly reactive oxygen species generated by Refs. [32,35]:

$$Ni^{2+} + O^{2-} + H_2 \rightarrow Ni^0 + H_2O + V_O$$
$$2Ce^{4+} + Ni^0 \rightarrow 2Ce^{3+} + Ni^{2+}$$

$$2Ce^{4+} + O^{2-} + H_2 \rightarrow 2Ce^{3+} + V_O + H_2O$$

where V_O indicates an oxygen vacancy in the lattice. For Pr-doped catalysts, an extra low temperature peak may be ascribed to the additional redox system:

$$Ni^{2+} + O^{2-} + H_2 \rightarrow Ni^0 + H_2O + V_O$$
$$2Pr^{4+} + Ni^0 \rightarrow 2Pr^{3+} + Ni^{2+}$$

$$2Pr^{4+} + O^{2-} + H_2 \rightarrow 2Pr^{3+} + V_O + H_2O$$

Please cite this article in press as: Iglesias I, et al., Ni/$Ce_{0.95}M_{0.05}O_{2-d}$ (M = Zr, Pr, La) for methane steam reforming at mild conditions, International Journal of Hydrogen Energy (2017), https://doi.org/10.1016/j.ijhydene.2017.09.176

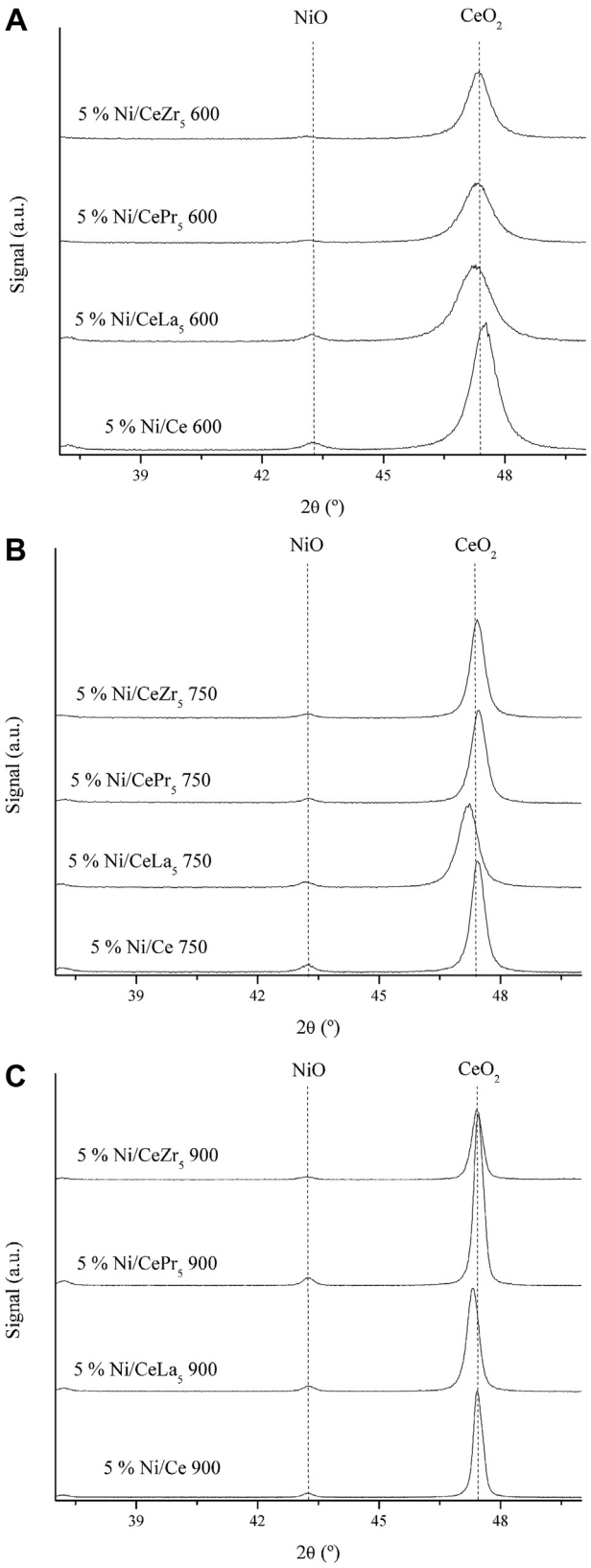

Fig. 1 – XRD patterns for catalysts' precursors calcined at 600 °C (A), 750 °C (B) and 900 °C (C).

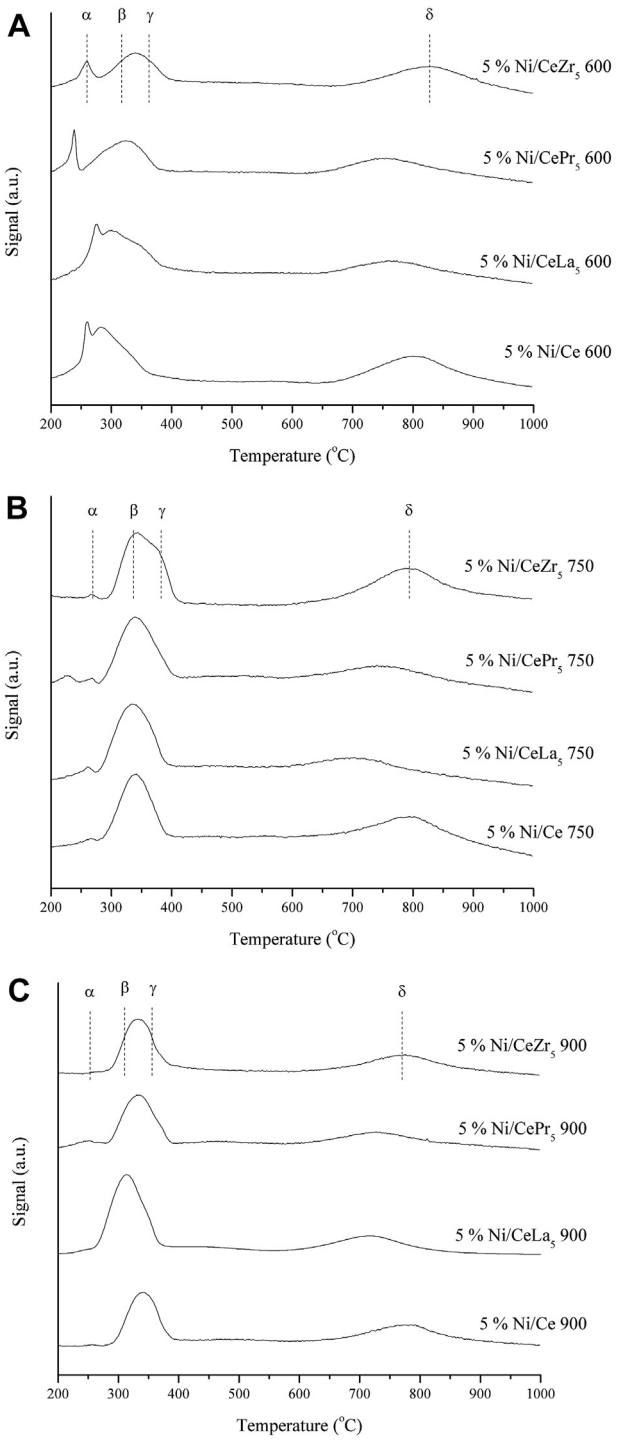

Fig. 2 – H_2-TPR profiles of catalysts calcined at 600 °C (A), 750 °C (B) y 900 °C (C).

In addition, there is some hydrogen consumption in the intermediate region, i.e. between peaks ϒ and δ, which Takeguchi et al. [35] attributed to nickel in intimate contact with the support by means of combined H_2-TPR and XRD analysis. When increasing calcination temperature, Peaks α and β presented lower hydrogen consumption while the opposite was true for peak ϒ, reinforcing its association to agglomerated nickel

Please cite this article in press as: Iglesias I, et al., $Ni/Ce_{0.95}M_{0.05}O_{2-d}$ (M = Zr, Pr, La) for methane steam reforming at mild conditions, International Journal of Hydrogen Energy (2017), https://doi.org/10.1016/j.ijhydene.2017.09.176

particles which are consistent with the metallic area decrease (see Table 2). Nevertheless, sample reduction still begun at lower temperatures in comparison to supports as characterized in previous work at the same conditions [24]. Most importantly, a maximum reducibility was observed for samples calcined at 750 °C which was interpreted as a consequence of increased nickel-ceria interaction. As it will be shown below, these samples had better catalytic performance in MSR.

Tables 1 and 2 show the results obtained for OSC and OSCC measurements, for supports and catalysts respectively, where the positive effect of doping ceria was observed. Doping ceria with trivalent cations such as La^{+3} generates intrinsic vacancies to maintain electroneutrality in the solid, vacancies which may favor oxygen mobility in the ceria lattice. However, since BET surface area diminution was observed (Table 1), OSC and OSCC values are almost the same for La doped and pure ceria. Zr-doped samples have no intrinsic vacancies generated as a consequence of cation substitution but, on the other hand, differences in cation size between Zr^{+4} and cerium generate lattice distortion which was proven to enhance oxygen mobility considerably [38]. In the case of praseodymium, previous results of our group had already exhibit an increase in oxygen mobility when doping ceria even with small quantities of Pr, both from experimental approach and DFT calculations [39]. Similar results were obtained by Ran et al. [40] when employing Ce-Zr-Pr samples, finding greatest oxygen mobility when using 5 at% of Pr.

For supports calcined at 600 °C, the greatest OSC and OSCC values were registered for Pr and Zr-doped ceria. Increasing calcination temperature was seen to produce a considerable decrement of specific surface area (Table 1) which, since OSC is identified as a surface phenomenon, has a negative effect on labile oxygen availability. OSC and OSCC for catalysts, shown in Table 2, were bigger than the ones for supports because of nickel ability to enhance oxygen mobility in the ceria lattice [41]. OSC increment due to nickel impregnation was almost the same for every sample and, consequently, Pr and Zr-doped catalysts were the ones with the higher values (as occurred with supports). On the other hand, relative differences between samples were somehow attenuated, in particular for 900 °C calcined ones, because Ni relevance is predominant over support. Therefore, catalysts' oxygen mobility decrease with calcination temperature may be associated not only to lower BET area but also to Ni agglomeration.

H_2-Chemisorption results are also shown in Table 2. In first place, it can be observed that nickel metallic area decreased with increasing calcination temperature as expected. Catalysts supported on $CePr_5$ were an exception to this diminution, which is in line with its particular behavior found in our previous work [24]. The decrease in nickel availability was lower for Zr and La-doped samples which were the supports with more stable BET surface areas. In addition, it can be noted that at every calcination temperature, the catalyst supported on zirconium doped ceria showed the highest metallic area. Additionally, it may be noticed that metallic area results were consistent with OSC measurements. It was observed an almost linear dependence of OSC and nickel metallic area for catalysts calcined at 900 °C, where support incidence in OSC value is expected to be negligible due to low surface area (see Fig. 3). This trend was not present with catalysts calcined at 600 °C and 750 °C suggesting that the support role in OSC measurement was relevant for those calcination temperatures.

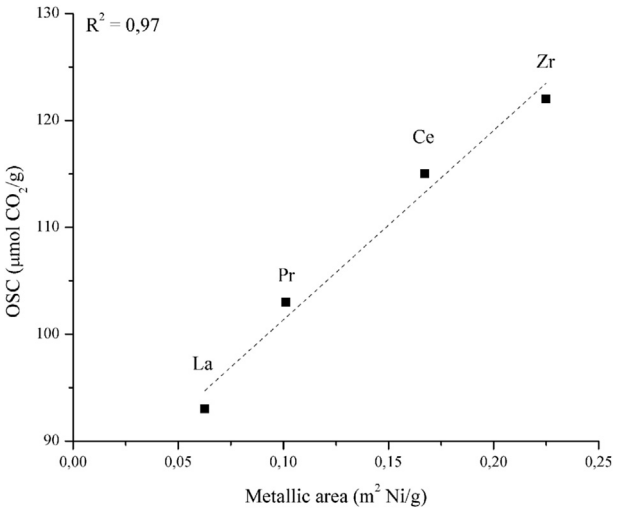

Fig. 3 – OSC versus metallic area for catalysts calcined at 900 °C (support dopant indicated).

Catalytic activity results

Table 4 shows the results for catalysts calcined at 900 °C and evaluated, with stoichiometric water/methane feed (R = 1), at different reaction temperatures: 600 °C, 700 °C and 800 °C in methane steam reforming. It was observed that the increase of reaction temperature had a positive effect on CO selectivity while CO_2 selectivity descended. Carbon monoxide and dioxide selectivities behavior may be explained by the exothermic water gas shift equilibrium displacement (Equation (2)) since this reaction is usually equilibrated in these reaction conditions [42]. Alternatively, this behavior could be understood in terms of the differences between labile and bulk oxygen roles in the reaction mechanism. Huang et al. [43] studied Gd-doped ceria and found that, in absence of any other oxygen source except for the support, CO_2 formation was related to superficial oxygen while CO formation was due to bulk activity. Since increasing temperature favors bulk oxygen mobility and surface area decrement, both effects may be responsible for the selectivities observed. Methane conversion increased with temperature at constant contact time, as expected, for every catalyst leading to similar hydrogen yields values. The increment in methane conversion was bigger from reaction temperature 600 to 700 °C than 700 to 800 °C, as previously reported by other authors [44,45]. As an example, Fig. 4 shows typical conversion and selectivities plots versus time on stream for 5% $Ni/CePr_5$ 900 while values in the tables hereinafter are all mean values.

Regarding these catalysts' deactivation, it may be observed that for activity tests at the highest temperature (800 °C), even though samples were calcined at 900 °C metal sintering is expected because of water vapor presence since it is known to enhance nickel mobility [46]. In fact it can be observed that deactivation ratio (ϕ) at 800 °C obeys the following trend for support's dopant: Zr > Ce > Pr > La, which is the same of the

Please cite this article in press as: Iglesias I, et al., $Ni/Ce_{0.95}M_{0.05}O_{2-d}$ (M = Zr, Pr, La) for methane steam reforming at mild conditions, International Journal of Hydrogen Energy (2017), https://doi.org/10.1016/j.ijhydene.2017.09.176

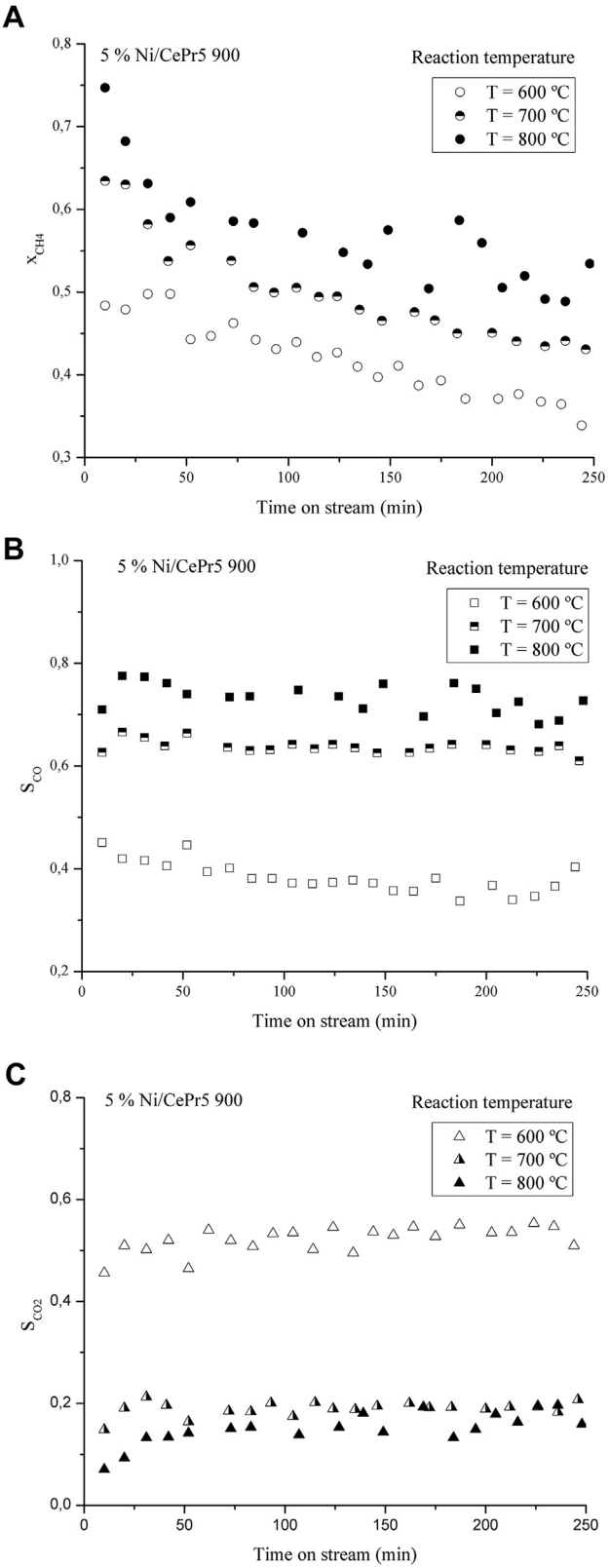

Fig. 4 – Methane conversion (circles), carbon monoxide selectivity (squares) and carbon dioxide selectivity (triangles) versus time on stream for 5% Ni/CePr$_5$ 900 at different reaction temperatures (R = 1, W/F = 1 g min/Nml).

metallic areas (see Table 2). This is explained considering that smaller particles are more prone to agglomeration. On the other hand, for activity tests at 600 °C, carbon formation was lower in accordance with Bartholomew [47].

Table 5 shows the results for catalysts calcined at 600 °C and evaluated at the same temperature with different water/methane feed ratios. It was observed that increasing water content at the feed resulted in greater carbon dioxide selectivity and lower carbon monoxide selectivity which is in agreement with literature [42] where this phenomenon is associated to water gas shift equilibrium displacement (Equation (2)). Once again, since higher vapor pressure enhances oxygen vacancies' replenishment, the increment of CO_2 selectivity may be interpreted as consequence of higher labile oxygen availability [19]. Regarding methane conversion, it was observed that, in the range evaluated, it increased with the increase of water content in the feed. The maximum observed for pure ceria supported catalyst may be explained in terms of water and methane competition for the same active site, as previously reported by other authors [48]. This maximum may be displaced to higher water/methane ratios for doped-support samples since water activation was reported to be facilitated [49]. Hydrogen yield, calculated by Equation (7), is a result of previous tendencies (methane conversion, CO and CO_2 selectivities) and has its highest values for R = 3 and doped samples. Reaction mechanisms presented in literature for metallic catalysts supported on oxides with redox activity suggest that water and the support itself serve as oxygen sources in the catalytic cycle [50]. At water deficient conditions, i.e. low water/methane feed ratio, main oxygen source will be the support. Accordingly, higher hydrogen yields are encountered in catalysts for which supports have higher OSC and OSCC values.

Two main deactivation causes in MSR are carbon formation and metal sintering. The first one is expected to prevail at low water/methane ratios while the second one is more likely to occur at high water partial pressures [51]. In line with this behavior, a minimum for deactivation ratio is predicted at an intermediate steam content which, as results in Fig. 5 show, occurred at R = 1.5 for samples employed in this work. For catalysts used at R = 3, Ni^0 crystallite diameter was estimated by XRD characterization after 4 h time on stream and these values are exhibited on Fig. 5 as well. At high water/methane ratios, deactivation ratio was higher for the catalysts with bigger Ni^0 particle diameter as expected if sintering was the main deactivation phenomenon. On the contrary, it may be observed that deactivation ratio at R = 0.5 is not perfectly correlated with carbon yield indicated in Fig. 5 (Y_C). Thus, to gain further insight into deactivation at this condition TPO analysis of these used samples was carried out and it is shown in Fig. 6. At least two types of carbon species are identified: one which is gasified at 530–580 °C (Type I) and other which is gasified at 600–650 °C (Type II, broken line in Fig. 6). The first type is associated to carbon in contact with nickel particles while the second one is ascribed to carbon over the support [52,53], for which its contribution to carbon yield is indicated. It is observed that this contribution obeys the following trend with sample dopant: Ce (none) > Pr > Zr > La which corresponds to deactivation observed suggestion that Type II

Please cite this article in press as: Iglesias I, et al., Ni/$Ce_{0.95}M_{0.05}O_{2-d}$ (M = Zr, Pr, La) for methane steam reforming at mild conditions, International Journal of Hydrogen Energy (2017), https://doi.org/10.1016/j.ijhydene.2017.09.176

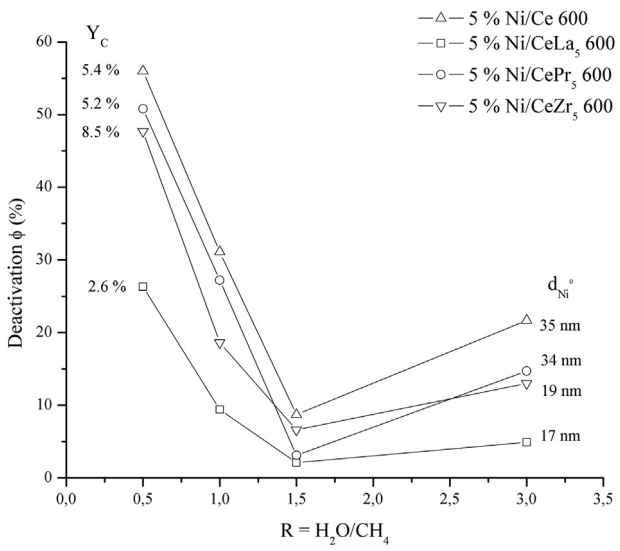

Fig. 5 – Deactivation as a function of water/methane feed ratio (R) for catalysts calcined at 600 °C (T = 600 °C, W/F = 1 g min/Nml, Time-on-stream = 4 h).

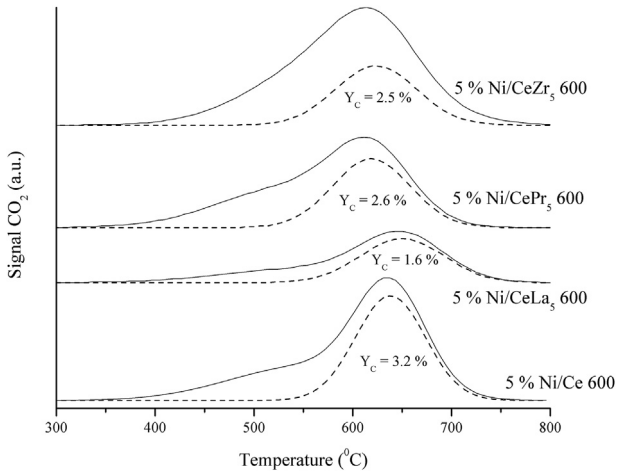

Fig. 6 – TPO profiles of catalysts calcined at 600 °C and used at R = 0.5, T = 600 °C, W/F = 1 g min/Nml, Time-on-stream = 4 h.

carbon is the one responsible for the catalysts' loss of activity in this reaction condition as expected [53,54].

Deactivation for pure ceria supported catalyst was the highest at every feed condition. It should be emphasized that, considering our reaction conditions, deactivation registered with R = 1.5 was extremely low for all catalysts compared to traditional Ni/Al_2O_3 catalysts.

In Table 6, activity results for catalysts calcined at different temperatures and tested at 600 °C and R = 1 are shown. It may be observed that maximum methane conversion was achieved for intermediate calcination temperature for every sample.

Higher calcination temperature diminishes nickel metallic area, i.e. increases nickel particle size, as previously discussed from data in Table 2. Despite some authors have found a positive dependence between Ni particle size and TOF for MSR [55,56], most careful studies done by Bengaard et al. [57] have proven that methane decomposition is favored on step sites, which in turn are more abundant on smaller crystallites. However, considering the results shown in Table 5 it is apparent that methane decomposition is not the sole rate determining step for these catalysts and, therefore, nickel-support interaction could be relevant in these system as previously suggested [12,36,43]. Dong et al. [36] found an optimum catalytic formulation based on Ni with intermediate metallic area where a good balance of two types of sites was achieved (one for methane activation, other one for water vapor activation). Roh et al. [12] made a similar observation but attributed the result to the presence of different oxidation states on nickel particles. For our catalysts, greater nickel-support interaction for 750 °C-calcined catalysts was observed by H_2-TPR. This increased reducibility produces higher oxygen vacancy concentration which is recognized as a key factor for MSR [43].

Conclusions

Catalysts prepared were characterized by several techniques (H_2-TPR, OSC, OSCC and H_2-Chemisorption) where support doping effects in enhancing nickel reducibility and its metallic area were observed. Zr-doped catalyst was the one to show the highest OSC and nickel availability.

To test reaction temperature effect on MSR, catalysts calcined at 900 °C were evaluated with R = 1 at 600, 700 and 800 °C. Deactivation was higher for these samples compared to the ones calcined at 600 °C and product distribution behavior was in agreement with WGS equilibrium displacement.

Catalysts calcined at 600 °C were tested in the MSR at mild conditions, ambient pressure, 600 °C and different water/methane feed ratios (R) below 3. Minimum deactivation was found for intermediate R values, which may be explained by coking and sintering competition. All doped-support catalysts showed lower deactivation in comparison to pure ceria supported samples. Zr-doped catalyst showed the best results both at water deficient conditions (R = 0.5), Y_{H2} = 23%, and high water content (R = 3), Y_{H2} = 70%.

Intermediate calcination temperature favored nickel-support interaction and sample reducibility, as observed by H_2-TPR. Despite having lower metallic area than 600 °C-calcined samples, catalysts calcined at 750 °C had the highest methane conversion in all the cases, regardless the support used.

Acknowledgments

Ignacio Iglesias is thankful to FIUBA for his Peruilh doctoral grant.

REFERENCES

[1] Laborde M, González FR. La Energía del Hidrógeno, CYTED, Buenos Aires-Oviedo. 2010.

Please cite this article in press as: Iglesias I, et al., $Ni/Ce_{0.95}M_{0.05}O_{2-d}$ (M = Zr, Pr, La) for methane steam reforming at mild conditions, International Journal of Hydrogen Energy (2017), https://doi.org/10.1016/j.ijhydene.2017.09.176

[2] Sinigaglia T, Lewiski F, Santos Martins ME, Mairesse Siluk JC. Production, storage, fuel stations of hydrogen and its utilization in automotive applications-a review. IJHE 2017. https://doi.org/10.1016/j.ijhydene.2017.08.063.
[3] Kuznetsov VL, David WIF, Brandon NP. Hydrogen and fuel cells: towards a sustainable energy future. Energy Policy 2008;36(12):4356–62.
[4] Rostrup-Nielsen J, Christiansen LJ. Concepts in syngas manufacture. London: Imperial College Press; 2011.
[5] Ashrafi M, Pfeifer C, Proll T, Hofbauer H. Experimental study of model biogas catalytic steam reforming: 2. Impact of sulfur on the deactivation and regeneration of Ni-Based catalysts. Energy Fuels 2008;22:4190–5.
[6] Grierson S, Strezov V, Ellem G, Mcgregor R, Herbertson J. Thermochemical conversion of microalgae: challenges and opportunities. J Anal Appl Pyrolysis 2009;85:118–23.
[7] Rostrup-Nielsen J. Catalysis, science and technology, vol. 5. Berlin: Springer-Verlag; 1984.
[8] Rostrup-Nielsen J, Bak Hansen J-H. CO_2 reforming of methane over transition metals. J Catal 1993;144:38–49.
[9] Turchetti L, Murmura MA, Monteleone G, Giaconia A, Lemonidou AA, Angeli SD, et al. Kinetic assessment of Ni-based catalysts in low-temperature methane/biogas steam reforming. IJHE 2016;41:16865–77.
[10] Dou B, Wang C, Song Y, Chen H, Xu Y. Activity of Ni–Cu–Al based catalyst for renewable hydrogen production from steam reforming of glycerol. Energy Convers Manag 2014;78:253–9.
[11] Lemonidou AA, Goula MA, Vasalos IA. Carbon dioxide reforming of methane over 5 wt% nickel calcium aluminate catalysts - effect of preparation method. Catal Today 1998;46:175–83.
[12] Roh H-S, Jun K-W, Park S-E. Methane-reforming reactions over Ni/Ce-ZrO_2/θ-Al_2O_3 catalysts. Appl Catal A General 2003;251:275–83.
[13] Großmann K, Treiber P, Karl J. Steam methane reforming at low S/C ratios for power-to-gas applications. IJHE 2016;41:17784–92.
[14] Angeli SD, Monteleone G, Giaconia A, Lemonidou AA. State-of-the-art catalysts for CH_4 steam reforming at low temperature. IJHE 2014;39:1979–97.
[15] Frusteri F, Freni S, Chiodo V, Donato S, Bonura G, Cavallaro S. Steam and auto-thermal reforming of bio-ethanol over MgO and CeO_2 Ni supported catalysts. IJHE 2006;31:2193–9.
[16] Huang T-J, Wang C-H. Roles of surface and bulk lattice oxygen in forming CO_2 and CO during methane reaction over gadolinia-doped ceria. Catal Lett 2007;118:103–8.
[17] Profeti LPR, Ticianelli EA, Assaf EM. Production of hydrogen via steam reforming of biofuels on Ni/CeO_2–Al_2O_3 catalysts promoted by noble metals. IJHE 2009;34:5049–60.
[18] Pompeo F, Gazzoli D, Nichio NN. Stability improvements of Ni/a-Al_2O_3 catalysts to obtain hydrogen from methane reforming. IJHE 2009;34:2260–8.
[19] Trovarelli A. Catalysis by ceria and related materials. London: Imperial College Press; 2002.
[20] Jobbágy M, Mariño F, Schönbrod B, Baronetti G, Laborde MA. Synthesis of copper-promoted CeO_2 catalysts. Chem Mater 2006;18:1945–50.
[21] Poggio E, Jobbágy M, Moreno M, Laborde M, Mariño F, Baronetti G. Influence of the calcination temperature on the structure and reducibility of nanoceria obtained from crystalline Ce(OH)CO_3precursor. IJHE 2011;18:15899–905.
[22] Yao HC, Yu Yao YF. Ceria in automotive exhaust catalysts: I. Oxygen storage. J Catal 1984;86:254–65.
[23] Hennings U, Reimert R. Stability of rhodium catalysts supported on gadolinium doped ceria under steam reforming conditions. Appl Catal A General 2008;337:1–9.
[24] Iglesias I, Baronetti G, Mariño F. Ceria and $Ce_{0.95}M_{0.05}O_{2-\delta}$ mixed oxides (M = La, Pr, Zr): vacancies and reducibility study. Solid State Ionics 2017. https://doi.org/10.1016/j.ssi.2017.07.008.
[25] Roh H-S, Eum I-W, Jeong D-W. Low temperature steam reforming of methane over Ni-$Ce_{(1-x)}Zr_{(x)}O_2$ catalysts under severe conditions. Renew Energy 2012;42:212–6.
[26] Lin K-H, Chang H-F, Chang ACC. Biogas reforming for hydrogen production over mesoporous $Ni_{2x}Ce_{1-x}O_2$ catalysts. IJHE 2012;37:15696–703.
[27] El-Kemary M, Nagy N, El-Mehasseb I. Nickel oxide nanoparticles: synthesis and spectral studies of interactions with glucose. Mater Sci Semicond Process 2013;16:1747–52.
[28] Mohammadyani D, Hosseini SA, Sadrnezhaad SK. Characterization of nickel oxide nanoparticles synthesized via rapid microwave-assisted route. Int J Mod Phys Conf Ser 2012;5:270–6.
[29] Huang T-J, Huang M-C. Effect of Ni content on hydrogen production via steam reforming of methane over Ni/GDC catalysts. Chem Eng J 2008;145:149–53.
[30] Radlik M, Adamowska-Teyssier M, Krzton A, Kozieł K, Krajewski W, Turek W, et al. Dry reforming of methane over Ni/$Ce_{0.62}Zr_{0.38}O_2$ catalysts: effect of Ni loading on the catalytic activity and on H_2/CO production. C R Chim 2015;18:1242–9.
[31] Vita A, Italiano C, Fabiano C, Lagan M, Pino L. Influence of Ce-precursor and fuel on structure and catalytic activity of combustion synthesized Ni/CeO_2 catalysts for biogas oxidative steam reforming. Mater Chem Phys 2015;163:337–47.
[32] Jalowiecki-Duhamel L, Zarrou H, D'Huysser A. Hydrogen production at low temperature from methane on cerium and nickel based mixed oxides. Int J Hydrogen Energy 2008;33:5527–34.
[33] Xu S, Yan X, Wan X. Catalytic performances of NiO-CeO_2 for the reforming of methane with CO_2 and O_2. Fuel 2006;85:2243–7.
[34] Solsona B, Concepción P, Hernández S, Demicol B, López-Nieto JM. Oxidative dehydrogenation of ethane over NiO-CeO_2 mixed oxides catalysts. Catal Today 2012;180:51–8.
[35] Takeguchi T, Furukawa S, Inoue M. Hydrogen spillover from NiO to the large surface area CeO_2–ZrO_2 solid solutions and activity of the NiO/CeO_2–ZrO_2 catalysts for partial oxidation of methane. J Catal 2001;202:14–24.
[36] Dong W-S, Roh H-S, Jun K-W, Park S-E, Oh Y-S. Methane reforming over Ni/Ce-ZrO_2 catalysts: effect of nickel content. Appl Catal A General 2002;226:63–72.
[37] Molina R, Poncelet G. α-Alumina-supported nickel catalysts prepared from nickel acetylacetonate: a TPR study. J Catal 1998;173:257–67.
[38] Bedrane S, Descorme C, Duprez D. Investigation of the oxygen storage process on ceria and ceria–zirconia-supported catalysts. Catal Today 2002;75:401–5.
[39] Poggio E, Irigoyen B, Baronetti G, Mariño F. Ce-Pr mixed oxides as active supports for water-gas shift reaction: experimental and density functional theory characterization. Appl Catal A Gen 2014;485:123–32.
[40] Ran R, Weng D, Wu X, Fan J, Wang L, Wu X. Structure and oxygen storage capacity of Pr-doped $Ce_{0.26}Zr_{0.74}O_2$ mixed oxides. J Rare Earths 2011;29:1053–9.
[41] Kacimi S, Barbier J, Taha R, Duprez D. Oxygen storage capacity of promoted Rh/CeO_2 catalysts. Exceptional behavior of RhCu/CeO_2. Catal Lett 1993;22:343–50.
[42] Xu J, Froment GF. Methane steam reforming, methanation and water gas shift: I. Intrinsic kinetics. AIChE J 1989;35:88–96.
[43] Huang T-J, Lin H-J, Yu T-C. A comparison of oxygen-vacancy effect on activity behaviors of carbon dioxide and steam reforming of methane over supported nickel catalysts. Catal Lett 2005;105(3–4):239–47.
[44] Kasza RV, Griffiths K, Shapter JG, Norton PR, Harrington DA. Interaction of water with stepped Ni(760): associative versus dissociative adsorption and autocatalytic decomposition. Surf Sci 1996;356:195–208.

Please cite this article in press as: Iglesias I, et al., Ni/$Ce_{0.95}M_{0.05}O_{2-d}$ (M = Zr, Pr, La) for methane steam reforming at mild conditions, International Journal of Hydrogen Energy (2017), https://doi.org/10.1016/j.ijhydene.2017.09.176

[45] Huang TJ, Yu TC. Effect of steam and carbon dioxide pretreatments on methane decomposition and carbon gasification over doped-ceria supported nickel catalyst. Catal Lett 2005;102(3–4):175–81.
[46] Sehested J, Gelten JAP, Remediakis IN, Bengaard H, Nørskov JK. Sintering of nickel steam-reforming catalysts: effects of temperature and steam and hydrogen pressures. J Catal 2004;223:432–43.
[47] Bartholomew CH. Carbon deposition in steam reforming and methanation. Catal Rev Sci Eng 1982;24(1):67–112.
[48] Elnashaie SSEH, Adris AM, Al-Ubaid AS, Soliman MA. On the non-monotonic behaviour of methane-steam reforming kinetics. Chem Eng Sci 1990;45(2):491–501.
[49] Halabi MH, de Croon MHJM, van der Schaaf J, Cobden PD, Schouten JC. Low temperature catalytic methane steam reforming over ceria–zirconia supported rhodium. Appl Catal A General 2010;389:68–79.
[50] Huang T, Lin H, Yu T. Effect of steam and carbon dioxide pretreatments on methane decomposition and carbon gasification over doped-ceria supported nickel catalyst. Catal Lett 2005;105:239–47.
[51] Sehested J. Four challenges for nickel steam-reforming catalysts. Catal Today 2006;111:103–10.
[52] Wang S, Lu GQM. CO_2 reforming of methane on Ni catalysts: effects of the support phase and preparation technique. Appl Catal B 1998;16:269–77.
[53] Gallezot P, Leclercq C, Barbier J, Marecot P. Location and structure of coke deposits on alumina-supported platinum catalysts by EELS associated with electron microscopy. J Catal 1989;116:164–70.
[54] Zhang ZL, Verykios XE. Carbon dioxide reforming of methane to synthesis gas over supported Ni catalysts. Catal Today 1994;21:589–95.
[55] Luisetto I, Tuti S, Battocchio C, Lo Mastro S, Sodo A. Ni/CeO_2–Al_2O_3catalysts for the dry reforming of methane: the effect of $CeAlO_3$ content and nickel crystallite size on catalytic activity and coke resistance. Appl Catal A General 2015;500:12–22.
[56] Christensen KO, Chen D, Lødeng R, Holmen A. Effect of supports and Ni crystal size on carbon formation and sintering during steam methane reforming. Appl Catal A General 2006;314:9–22.
[57] Bengaard HS, Nørskov JK, Sehested J, Clausen BS, Nielsen LP, Molenbroek AM, et al. Steam reforming and graphite formation on Ni catalysts. J Catal 2002;209:365–84.

Please cite this article in press as: Iglesias I, et al., Ni/$Ce_{0.95}M_{0.05}O_{2-d}$ (M = Zr, Pr, La) for methane steam reforming at mild conditions, International Journal of Hydrogen Energy (2017), https://doi.org/10.1016/j.ijhydene.2017.09.176